PARAMETRIC SAR IMAGE FORMATION - A PROMISING APPROACH TO RESOLUTION-UNLIMITED IMAGING

Yesheng Gao, Kaizhi Wang, Xingzhao Liu

Shanghai Jiao Tong University
Department of Electronic Engineering
ysgao@sjtu.edu.cn

ABSTRACT

A parametric SAR image formation scheme is proposed in this paper. Based on a model describing the received signal, the parameters of the model can be used to characterize the illuminated scene. A realization of parameter estimation via atomic decomposition is presented. The estimated parameters are then mapped onto the iso-range-Doppler grid to form a SAR image. Simulation results demonstrate that this scheme can provide an approach to resolution-unlimited imaging.

Index Terms— Synthetic aperture radar (SAR), image formation, parameter estimation, atomic decomposition

1. INTRODUCTION

Synthetic aperture radar (SAR) uses the relative motion between an antenna and the illuminated scene to form high resolution images. The antenna is usually mounted on a moving platform, including aircraft and spacecraft [1].

Conventional SAR imaging algorithms have been developed based on the data collection geometries. The range resolution is constrained by the transmitted signal bandwidth, while the azimuth resolution is determined by the synthetic aperture length or the synthetic angle.

SAR image formation can also be viewed as a parameter estimation problem [2]. DeGraaf discussed SAR image formation using modern 2-D spectral estimation methods, and gave a comprehensive comparison of these methods [2]. Gerry proposed a parametric model for radar scattering in two dimensions, and presented an approximate maximum likelihood (ML) algorithm for estimating the parameters [3]. Li gave a model of the signal reflected from dihedrals and trihedrals, and implemented image formation and target feature extraction using spectral estimation methods [4, 5].

We present a parametric SAR image formation scheme in this paper. Using a point scatterer assumption, a parametric model is used to describe the SAR signal. Each scatterer is characterized by a set of parameters, and the parameters are estimated by signal processing tools. We take atomic decomposition as an example for parameter estimation to demonstrate the feasibility of the proposed scheme.

The remainder of this paper is organized as follows. In section II, the fundamentals of SAR imaging are reviewed. In section III, the model of the SAR signal is introduced. In section IV, a realization of the proposed parametric SAR imaging scheme is discussed. Atomic decomposition is used to estimate parameters, which is mapped to form a SAR image. In section V, simulation results are given. A summary is concluded in section VI.

2. FUNDAMENTALS OF SAR IMAGING

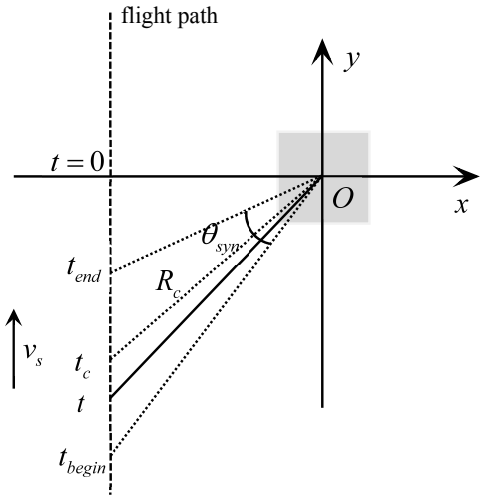

Fig. 1. Geometry of SAR Data collection.

The data collection geometry is illustrated in Fig. 1. The plane constituted by the flight path and the scene center is labeled as an x-y Cartesian coordinate system. The origin of the coordinate system, O, is at the scene center. Assume that $t = 0$ is the time of closest approach, azimuth time from $t_{\rm begin}$ to $t_{\rm end}$ is a coherent processing aperture, $t_{\rm c}$ denotes the azimuth time evaluated at the aperture center. The instantaneous slant range $R(t)$ can be expressed as

$$R(t) = \sqrt{R_{\rm c}^2 - (v_{\rm s}t_{\rm c})^2 + (v_{\rm s}t)^2} \qquad (1)$$

where v_s is the platform velocity, R_c is the distance between the antenna phase center (APC) and the target at $t = t_c$.

The spatial resolution in the range dimension is

$$\rho_r = K_r \frac{c}{2B} \tag{2}$$

where c is light velocity, B is the bandwidth of the transmitted signal. K_r is a mainlobe broadening factor introduced by the aperture weighting function used for sidelobe control and by any low-frequency phase errors present in the signal.

The expression for azimuth resolution is

$$\rho_a = K_a \frac{\lambda}{2\theta_{syn}} \tag{3}$$

where λ is the wavelength, θ_{syn} is the angle during which the target is illuminated in the coherent processing aperture. K_a is a mainlobe broadening factor introduced by aperture weighting for sidelobe control of the system impulse response and by residual amplitude and phase errors.

The area determined by ρ_r and ρ_a is defined as *resolution cell*. SAR receives the signal reflected from many resolution cells simultaneously, but is able to separate the returns from each resolution cell by using image formation algorithms. Conventional algorithms have been developed based on data collection geometries, and Fourier transform provides a chance of their effective implementations. Such algorithms include range-Doppler algorithm (RDA), chirp scaling algorithm (CSA), polar format algorithm (PFA) and ω-k algorithm (ωkA).

3. MODEL OF THE SAR SIGNAL

Unlike conventional image formation algorithms, we desire to present a parametric image formation scheme. In this section, the model of the SAR signal is described. We concentrate on azimuth signal focusing, the method of parameter estimation discussed in the next section can be extended to range dimension straightforwardly.

After demodulation, the signal reflected from a point scatterer can be written as

$$\begin{aligned} s(\tau, t) =& A\omega_r\left(\tau - \frac{2R(t)}{c}\right)\omega_a(t - t_c) \\ & \times e^{-j\pi k_r\left(\tau - \frac{2R(t)}{c}\right)^2} e^{-j\frac{4\pi}{\lambda}R(t)} \end{aligned} \tag{4}$$

where τ and t are fast and slow time, $\omega_r(\cdot)$ and $\omega_a(\cdot)$ are the range and azimuth envelope, A is a constant, k_r is the chirp rate of transmitted signal. The range-compressed signal is

$$s(t) = Ap_r\left(\tau - \frac{2R(t)}{c}\right)\omega_a(t - t_c)e^{-j\frac{4\pi}{\lambda}R(t)} \tag{5}$$

where $p_r(\cdot)$ is the range-compressed envelope. $R(t)$ is calculated using equation (1). According to the actual physical procedure of SAR imaging, a mathematical function can be used to fit $R(t)$, and then a model of the signal can be constructed. $R(t)$ is approximated by

$$R_p(t) = R_c + a_1(t - t_c) + a_2(t - t_c)^2 + \cdots . \tag{6}$$

The model of the SAR signal can be expressed as

$$s_p(t; \boldsymbol{\theta}_p) = Ap_r(\tau - \frac{2R_p(t)}{c})\omega_a(t - t_c)e^{-j\frac{4\pi}{\lambda}R_p(t)} \tag{7}$$

where $\boldsymbol{\theta}_p = [T, t_c, a_1, a_2, \cdots]$, T denotes the temporal support of $\omega_a(\cdot)$. The signal can be focused in azimuth by estimating $\boldsymbol{\theta}_p$.

The order of the polynomial in (7) is determined by the relationship between the resolution and the geometric error. That is, it is determined by whether or not the difference between the actual and the presumed geometry is comparable to the spatial resolution. Generally, the finer the spatial resolution is, the higher the order of the polynomial needed.

The signal model of a group of point scatterers can be written as

$$\begin{aligned} s_\Sigma(t; \boldsymbol{\theta}_p^i) &= \sum_i s_p^i(t) \\ &= \sum_i A^i p_r^i\left(\tau - \frac{2R_p^i(t)}{c}\right)\omega_a^i(t - t_c^i)e^{-j\frac{4\pi}{\lambda}R_p^i(t)}. \end{aligned} \tag{8}$$

These scatterers can be reconstructed one by one in a SAR image.

4. ATOMIC DECOMPOSITION-BASED IMAGE FORMATION ALGORITHM

4.1. Parameter estimation

In this section, we give a realization of the parametric image formation scheme. The parameters are estimated via atomic decomposition (AD) [6, 7]. A dictionary is constructed to implement the AD. Each atom in the dictionary is unity energy and has the form as below.

$$a(t; \boldsymbol{\theta}_p) = \frac{1}{\sqrt{T}}\mathrm{rect}(\frac{t - t_c}{T})e^{-j\frac{4\pi}{\lambda}R_p(t)}. \tag{9}$$

To estimate $\boldsymbol{\theta}_p$, a cost function named matching degree indicator (MDI) is defined as

$$\mathcal{M}(\boldsymbol{\theta}_p) = \left|\int_{t_c - T/2}^{t_c + T/2} \overline{s\left(t, R(\boldsymbol{\theta}_p)\right)}\, a^*(t; \boldsymbol{\theta}_p)\, dt\right|^2 \tag{10}$$

where $s\left(t, R(\boldsymbol{\theta}_{\mathrm{p}})\right)$ is the range-compressed signal along RMC $R(\boldsymbol{\theta}_{\mathrm{p}})$, and $\overline{s\left(t, R(\boldsymbol{\theta}_{\mathrm{p}})\right)}$ is the form with its energy normalized to unity.

Each $\boldsymbol{\theta}_{\mathrm{p}}$ can be used to calculate a range migration curve (RMC). The parameter estimation can be regarded as a procedure of finding the RMC along which the signal can match the model best. That is, it is to find the $\boldsymbol{\theta}_{\mathrm{p}}^{\dagger}$ maximizing equation (9). The parameter estimation is demonstrated in Fig. 2.

The best-matched parameter vector $\boldsymbol{\theta}_{\mathrm{p}}^{\dagger}$ can be obtained by

$$\boldsymbol{\theta}_{\mathrm{p}}^{\dagger} = \arg\max \mathcal{M}(\boldsymbol{\theta}_{\mathrm{p}}). \tag{11}$$

The intensity of the scatterer present in the final SAR image is

$$A_{\mathrm{in}} = Q \cdot \mathcal{M}(\boldsymbol{\theta}_{\mathrm{p}}^{\dagger}) \tag{12}$$

where

$$Q = \left| \int_{t_{\mathrm{c}}-T/2}^{t_{\mathrm{c}}+T/2} s\left(t, R(\boldsymbol{\theta}_{\mathrm{p}}^{\dagger})\right) s^{*}\left(t, R(\boldsymbol{\theta}_{\mathrm{p}}^{\dagger})\right) \, \mathrm{d}t \right|^{2}. \tag{13}$$

The best-matched parameter vector $\boldsymbol{\theta}_{\mathrm{p}}^{\dagger}$ is estimated as follows.

Step 1: Construct the dictionary of atoms with parameter vectors $\{\boldsymbol{\theta}_{\mathrm{p}}\}$.

Step 2: Calculate the range migration $R(\boldsymbol{\theta}_{\mathrm{p}})$ of each $\boldsymbol{\theta}_{\mathrm{p}}$ in the dictionary according to equation (6).

Step 3: Search over the data matrix for the best-matched parameter vector $\boldsymbol{\theta}_{\mathrm{p}}^{\dagger}$ using equation (11).

Step 4: The intensity of the scatterer is obtained using equation (12).

The parameter estimation can be continued until the residual energy is over $\mathcal{E}_{\mathrm{th}}$ or the achieved MDI is below $\mathcal{M}_{\mathrm{th}}$. We assume that the obtained $\boldsymbol{\theta}_{\mathrm{p}}^{\dagger}$ in each iteration corresponds to a point scatterer, which is reconstructed in the final SAR image.

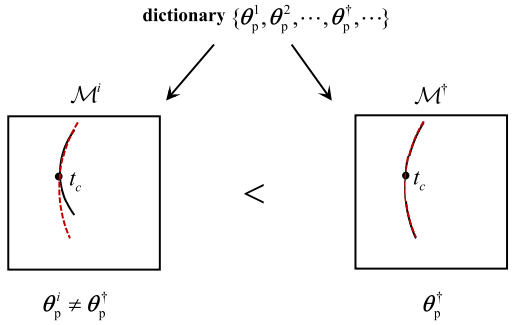

Fig. 2. Procedure of parameter estimation.

4.2. parameter mapping

SAR image can be viewed as a projection of the scene radar cross section (RCS) onto the grid formed by iso-range and iso-Doppler contours in the ground plane [1]. For a SAR radar flying along an ideal trajectory, a constant-range sphere is the sphere centered at the APC. Constant-range spheres intersect the flat ground plane as circles centered at the APC nadir point, marked as the solid black circle in Fig. 3. Each of these circles is called *iso-range line*, as the dashed lines in Fig. 3. The scatterers placed on the same iso-range line have the same distance to the APC. A constant Doppler surface is the conical surface with apex at the APC. Constant-Doppler cones intersect the flat ground plane as hyperbolas. Each of these hyperbolas is called *iso-Doppler line*, as the solid lines in Fig. 3. The scatterers placed on the same iso-Doppler line have the same Doppler centroid. The image grid is formed by these two sets of lines and is called iso-range-Doppler grid.

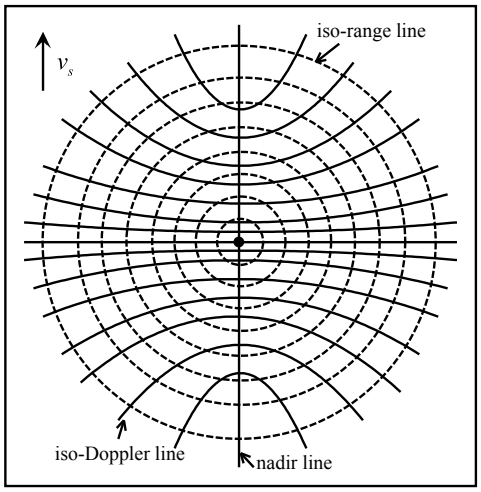

Fig. 3. Grid formed by iso-range and iso-Doppler lines.

In the AD-based image formation algorithm, a SAR image is formed by mapping the estimated parameters onto the grid. The azimuth position of a scatterer is determined by its Doppler centroid, i.e., $f_{\mathrm{c}} = -\frac{2}{\lambda} a_1$. The intensity of the scatterer A_{in} is obtained in Step 4 of the parameter estimation.

5. SIMULATION RESULTS

5.1. Image formation of a single scatterer

The primary parameters are listed in Table 1. The point scatterer is placed at the center of the illuminated scene. In this simulation, we adopted quadratic phase in equation (9). Fig. 4 is the imaging result with $\mathcal{E}_{\mathrm{th}} = 2\%$ of the original energy. Fig. 5 is the imaging result with $\mathcal{E}_{\mathrm{th}} = 5\%$ of the original energy. In both simulations, $\mathcal{M}_{\mathrm{th}}$ is set at 0.8. The graphic processing unit (GPU) is used in the calculation owing to its powerful parallel computation capability [8].

In Fig. 5, the point scatterer is characterized by a single parameter vector, thus it is reconstructed as a pixel in the final image. When $\mathcal{E}_{\mathrm{th}}$ decreased to 2% of the original energy,

Table 1. Simulation parameters

Parameter	Value
Wavelength	0.03125 m
Bandwidth	800 MHz
Pulse length	10 μs
PRF	1000 Hz
Platform velocity	100 m/s

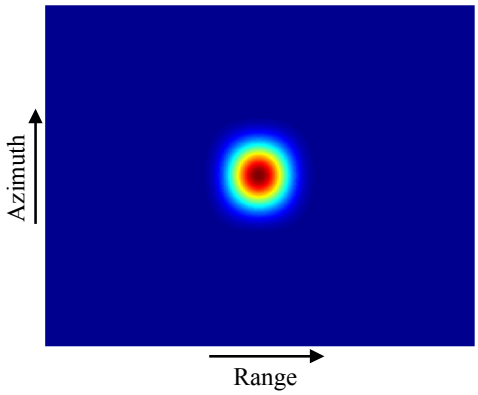

Fig. 4. Imaging result ($\mathcal{E}_{\text{th}} = 2\%$ of the original energy).

more parameter vectors can be estimated, the corresponding intensity of the second parameter vector is -35 dB below the first one. This results from the estimation error by using the signal model. Unlike the conventional SAR images, the parametric image formation scheme can generate resolution-unlimited images. Strictly speaking, resolution-unlimited imaging can be considered the SAR image is formed by reconstructing scatterer(s) by scatterer(s). The resultant image is suitable for target detection and feature extraction, although it may not be visually satisfactory.

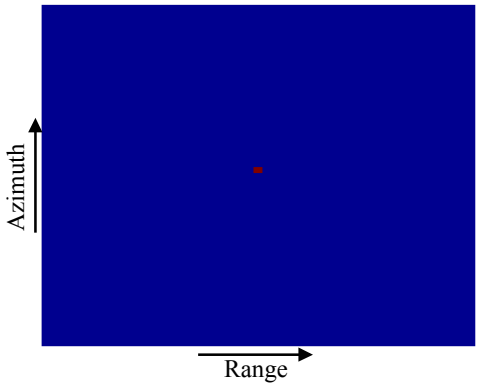

Fig. 5. Imaging result ($\mathcal{E}_{\text{th}} = 5\%$ of the original energy).

5.2. Image formation of multi-targets

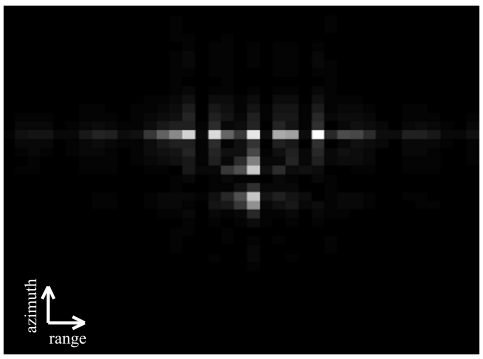

Fig. 6. Image formed using the CSA.

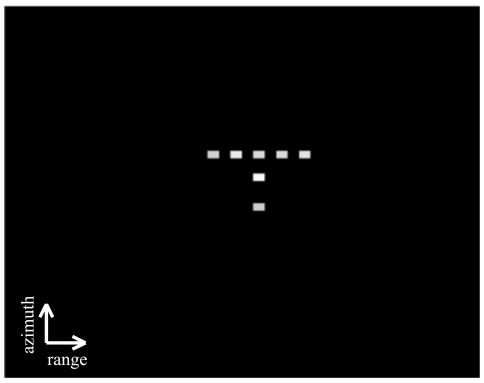

Fig. 7. Image formed using AD-based algorithm.

In this simulation, seven point targets are placed into the letter "T", and the space of two adjacent point targets is twice the range resolution. The key parameters of radar system are listed in Table 1, quadratic phase is also adopted. In this simulation, $\mathcal{E}_{\text{th}}$ is set at 5% of the original energy, and $\mathcal{M}_{\text{th}}$ is set at 0.8. Fig. 6 shows an image made using the chirp scaling algorithm [9]. An image made using the AD-based imaging algorithm is shown in Fig. 7. The image quality of Fig. 6 is deteriorated due to the mainlobe and sidelobe effects, which is an intrinsic drawback of Fourier SAR imaging. In Fig. 7, over 95% of a target's energy is concentrated on a pixel of the image.

6. CONCLUSION

We present a parametric SAR image formation scheme in this paper and give its realization via atomic decomposition. With the assumption of point scatterer, each set of model parameters is estimated to characterize a single scatterer. From the simulation results, a point scatterer can be presented as a single pixel in the final image. That is, the resolution is

not constrained by the radar system and the synthetic aperture length as the conventional algorithms do. However, the AD-based algorithm is more computationally complex than the conventional ones. Our further work will concentrate on algorithm structure and performance optimization.

7. REFERENCES

[1] Walter G. Carrara, Ronald M. Majewski, and Ron S. Goodman, *Spotlight Synthetic Aperture Radar: Signal Processing Algorithms*, Artech House, July 1995.

[2] S.R. DeGraaf, "SAR imaging via modern 2-D spectral estimation methods," *IEEE Transactions on Image Processing*, vol. 7, no. 5, pp. 729 – 761, May 1998.

[3] M.J. Gerry, L.C. Potter, I.J. Gupta, and A. Van Der Merwe, "A parametric model for synthetic aperture radar measurements," *IEEE Transactions on Antennas and Propagation*, vol. 47, no. 7, pp. 1179 – 1188, Jul. 1999.

[4] Renbiao Wu, Jian Li, Zhaoqiang Bi, and P. Stoica, "SAR image formation via semiparametric spectral estimation," *IEEE Transactions on Aerospace and Electronic Systems*, vol. 35, no. 4, pp. 1318 – 1333, Oct. 1999.

[5] Zhaoqiang Bi, Jian Li, and Zheng-She Liu, "Super resolution SAR imaging via parametric spectral estimation methods," *IEEE Transactions on Aerospace and Electronic Systems*, vol. 35, no. 1, pp. 267 – 281, Jan. 1999.

[6] O.A. Yeste-Ojeda, J. Grajal, and G. Lopez-Risueno, "Atomic decomposition for radar applications," *IEEE Transactions on Aerospace and Electronic Systems*, vol. 44, no. 1, pp. 187 – 200, Jan. 2008.

[7] A. Bultan, "A four-parameter atomic decomposition of chirplets," *IEEE Transactions on Signal Processing*, vol. 47, no. 3, pp. 731 – 745, Mar. 1999.

[8] J.D. Owens, M. Houston, D. Luebke, S. Green, J.E. Stone, and J.C. Phillips, "GPU computing," *Proceedings of the IEEE*, vol. 96, no. 5, pp. 879 – 899, May 2008.

[9] R.K. Raney, H. Runge, R. Bamler, I.G. Cumming, and F.H. Wong, "Precision SAR processing using chirp scaling," *IEEE Transactions on Geoscience and Remote Sensing*, vol. 32, no. 4, pp. 786 – 799, Jul. 1994.